Initial Observations With Electronic and Mechanical Scans Using a Cylindrical Polarimetric Phased Array Radar

Zhe Li, *Student Member, IEEE*, Guifu Zhang, *Senior Member, IEEE*, Mohammad-Hossein Golbon-Haghighi, *Student Member, IEEE*, Hadi Saeidi-Manesh, *Member, IEEE*, Matthew Herndon, *Student Member, IEEE*, and Hong Pan

***Abstract*— This letter presents initial weather measurements with a cylindrical polarimetric phased array radar (CPPAR) demonstrator developed at The University of Oklahoma. The overall system specifications, waveform design, beam pattern measurement, and beam-to-beam calibration of the CPPAR demonstrator are presented. The weather observations of convective precipitation are provided, employing a single-beam mechanical scan and commutating beam electronic scan. Measurement results from these two scan modes are compared, and the error statistics are derived and discussed. A new feature of the CPPAR commutating beam electronic scan in clutter detection is observed and explained.**

***Index Terms*— Clutter detection, commutating beam, cylindrical polarimetric phased array radar (CPPAR), electronic scan, weather measurements.**

I. Introduction

In RECENT years, phased array radar (PAR) technology has received much attention in the weather community, owing to its capability of faster data updates and the potential to serve multiple missions. On the other hand, weather radar polarimetry has matured in applications such as hydrometeor classification, quantitative precipitation estimation, attenuation correction, microphysics retrieval, and so on. Therefore, a desirable candidate for future weather observation is a polarimetric PAR (PPAR) [1], which is capable for both the polarimetry of multiparameter measurements and the fast-scan proficiency of the PAR.

Manuscript received July 13, 2019; revised October 28, 2019; accepted January 29, 2020. Date of publication March 9, 2020; date of current version January 21, 2021. This work was supported by the National Oceanic and Atmospheric Administration (NOAA) under Grant NA16OAR4320115. *(Corresponding author: Zhe Li.)*

Zhe Li, Mohammad-Hossein Golbon-Haghighi, and Hadi Saeidi-Manesh are with the School of Electrical and Computer Engineering, The University of Oklahoma, Norman, OK 73019 USA, and also with the Advanced Radar Research Center, The University of Oklahoma, Norman, OK 73019 USA (e-mail: zhe.li-1@ou.edu; golbon@ou.edu; hadi.saeidimanesh@ou.edu).

Guifu Zhang is with the School of Meteorology, The University of Oklahoma, Norman, OK 73072 USA, and also with the School of Electrical and Computer Engineering and Advanced Radar Research Center, The University of Oklahoma, Norman, OK 73019 USA (e-mail: guzhang1@ou.edu).

Matthew Herndon and Hong Pan are with the Advanced Radar Research Center, The University of Oklahoma, Norman, OK 73019 USA (e-mail: mherndon@ou.edu; hpan@ou.edu).

Color versions of one or more of the figures in this letter are available online at https://ieeexplore.ieee.org.

Digital Object Identifier 10.1109/LGRS.2020.2971471

However, it is challenging to collect high-quality polarimetric radar data of weather with a PPAR. For example, with a planar PPAR (PPPAR), the beam and polarization characteristics change with the electronic beam direction, causing geometrically induced cross-polarization coupling [1]–[4], as well as sensitivity losses and measurement biases when the PPPAR beam is steered away from the broadside [5], which imposes a lot of difficulties for calibration and accurate polarimetric weather measurements.

To overcome the inherent deficiencies of PPPAR, the concept of cylindrical polarimetric PAR (CPPAR) was proposed for future weather measurements and multiple missions [5]. In a CPPAR system, beam steering in the azimuth is realized by a commutating scan, in which the beam direction changes in the azimuth by shifting a column of excited antenna sector and maintaining the weight symmetry about the beam center. As a result, the CPPAR has scan-invariant beam characteristics in the azimuth and polarization purity in all directions, which allows for high-quality polarimetric weather measurements. To validate the CPPAR concept, a small-scale CPPAR demonstrator has been jointly developed by the Advanced Radar Research Center (ARRC) at The University of Oklahoma (OU) and the National Severe Storms Laboratory of NOAA [6]–[8]. Initial weather measurements were made in the summer of 2019.

This letter presents the results of these initial weather measurements to show the performance of the CPPAR demonstrator and polarimetric data quality that could be achieved by a cylindrical array radar. Section II describes the engineering design and specifications of the CPPAR demonstrator, including system overview, waveform design, beamforming, and pattern measurements, as well as beam-to-beam calibration. Section III presents the weather measurements of a convective precipitation made with the CPPAR, employing the single-beam mechanical scan and commutating beam electronic scan. The measurements are compared qualitatively with KTLX, a nearby operational next-generation radar (NEXRAD); then, a quantitative comparison is made between the two scan modes, and error statistics are estimated and discussed. Section IV explores and verifies a feature of the commutating beam electronic scan in clutter detection. Section V summarizes these results and discusses future improvements to the CPPAR demonstrator.

Fig. 1. CPPAR demonstrator. (a) On the ground. (b) Moved to ARRC rooftop.

TABLE I
TECHNICAL SPECIFICATIONS OF THE CPPAR DEMONSTRATOR

Radar Parameters	Values
Frequency	2.7~3.0 GHz
Waveform	LFM/NLFM
Pulse Width	1~100 μs
Pulse Repetition Time	1~100 ms
Antenna Element	Patch
Beamwidth	Azimuth: 6.20°, Elevation: 5.35°
Sidelobes	≤-28 dB
Polarization	Dual polarization
Peak Power	180 W per column
Dynamic Range	74 dB
Noise Figure	2.8 dB
Bandwidth	1~5 MHz
Range Resolution	30~150 m

II. ENGINEERING DESIGN AND SPECIFICATIONS OF THE CPPAR DEMONSTRATOR

A. System Overview

As shown in Fig. 1, the CPPAR demonstrator consists of a cylinder with a diameter of 2-m and a height of 2-m, in which there is a server for system control and communication. The cylinder is fully populated with 96 columns of subarrays, whereas currently only 48 of these columns have been equipped with channel electronics. Each column is a 19-element linear array of dual-polarization, frequency-scanned, microstrip patch antenna, which is designed to operate over a frequency range from 2.7 to 3.0 GHz, corresponding to a scanning range from 0° to 20° in elevation [6], [9]. The spacing between the columns on the cylinder is 6.5 cm, equivalent to an azimuthal angle of 3.75°. Feed networks are designed to perform analog beamforming while doing commutating scans in azimuth. The technical specifications of the CPPAR demonstrator are shown in Table I.

B. Waveform Design

On transmit, the AD9361 radio frequency (RF) transceiver uses a baseband synthesizer for waveform generation, including linear frequency modulation (LFM) waveform, nonlinear frequency modulation (NLFM) waveform, and so on. Based on the maximum sampling rate and available taps of the matched filter in the RF transceiver, an optimized NLFM pulse compression waveform is designed by following the genetic algorithm documented in [10] and implemented in CPPAR. As shown in Fig. 2, the optimized NLFM waveform has a maximum pulsewidth of 34 μs, peak sidelobe level below -63 dB, and integrated sidelobe level below -41 dB, as well as a power efficiency of 93.66% and a 3-dB range resolution of 80 m.

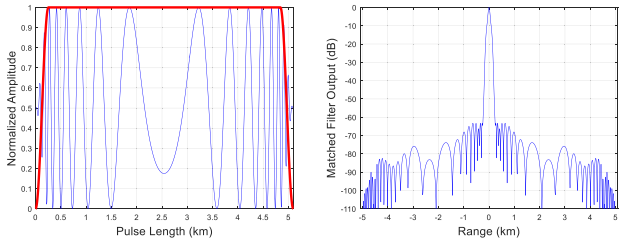

Fig. 2. NLFM waveform in CPPAR. (a) Real component. (b) Autocorrelation function.

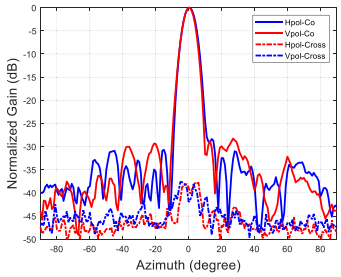

Fig. 3. CPPAR optimized beam patterns.

C. Pattern Measurement and Optimization

To demonstrate the advantages of CPPARs in polarization purity and azimuth scan-invariant beam characteristics, CPPAR beam patterns are measured by a calibration horn mounted on the National Weather Center which is about 225 m away from the CPPAR. The horn height can be adjusted based on the CPPAR beam steering elevation, which is determined by the frequency of operation. At the frequency of 2.76 GHz, the CPPAR points at 3.3° in elevation, and the horn is mounted at approximately 13 m above the CPPAR. First, all the azimuthal element (column) radiation patterns are measured. As in [11], a multiobjective optimization method is used to find the optimum weights to form the beams from the center of each active 90° sector (24 columns) of the cylinder. The goal is to match the copolar patterns between horizontal and vertical polarizations for all commutating beams while maintaining the sidelobe levels and maximizing the gain. Fig. 3 shows the optimized horizontal and vertical polarization beam patterns of an active 90° sector of CPPAR, which have the sidelobe levels lower than -28 dB (one-way), and the cross-polarization levels are below -37 dB from the copolar peak.

D. System Calibration

In the electronic scan mode, the beamforming weights optimized from the central sector (Column No.13~36) are applied to all the commutating sectors for beamforming. Due to the variations in element (column) pattern and channel electronics (attenuator, phase shifter, etc.), the calibration factor (radar constant) may be slightly different from beam to beam. To calibrate, two step procedures are implemented in the CPPAR demonstrator. The first step is to obtain radar constant

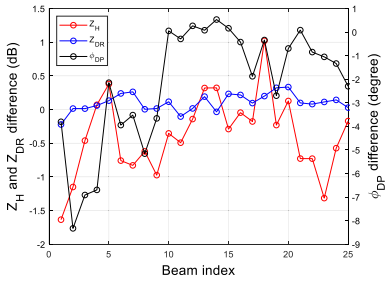

Fig. 4. Mean differences between electronic scan and mechanical scan for CPPAR calibration.

for the single beam formed by the central sector. According to the weather radar equation [12]

$$Z = P_r + C + 20\log_{10} R \tag{1}$$

based on CPPAR specifications, radar constant is obtained as $C = 98.14$ dB and verified by comparison with KTLX measurements. Since the CPPAR and KTLX have very different resolutions and are not collocated, the verification just shows the consistency of the CPPAR. The second step is to compensate for the beam-to-beam variation based on weather measurements, which uses the differences between electronic scan and mechanical scan from the previous measurements to calibrate the measurements of the current electronic scan. The mean differences for reflectivity (Z_{H}), differential reflectivity (Z_{DR}), and differential phase (ϕ_{DP}) used for calibration are shown in Fig. 4. The Z_{H} differences are typically within 1.0 dB, Z_{DR} differences are less than 0.3 dB, and the ϕ_{DP} differences are mostly within 5.0°. This shows the advantage of the scan-invariant commutating beam of the CPPAR, simplifying the calibration for polarimetric measurements. Nevertheless, these small differences were corrected from the previous experiment, and after correction, the electronic scan measurements become more consistent, as shown in Section III.

III. Weather Measurements

During the summer of 2019, CPPAR was operated for testing and initial weather measurements, using the single-beam mechanical scan and commutating beam electronic scan, respectively, when the data sets of the two scans were collected 24 s apart. The main scanning parameters during data collection are shown in Table II. To reduce noise effects, the one-lag estimator was employed in pulse-pair processing [13]. In addition, a notched filter was employed to mitigate the clutter effect on weather measurements. Weather measurements including reflectivity, radial velocity (v_{r}), spectrum width (σ_{v}), differential reflectivity, copolar correlation coefficient (ρ_{hv}), and differential phase in a convective precipitation case are shown in Fig. 5. For qualitative comparison, observations from the nearby KTLX are also shown in Fig. 5 as reference. As can be seen, the CPPAR electronic scan visually produces almost the same measurements as its mechanical scan. Moreover, CPPAR measurements are generally consistent with KTLX observations except for the difference in resolution. It should be noted that the difference in v_{r} and ϕ_{DP} measurements is because the resolution volumes in precipitation are seen by

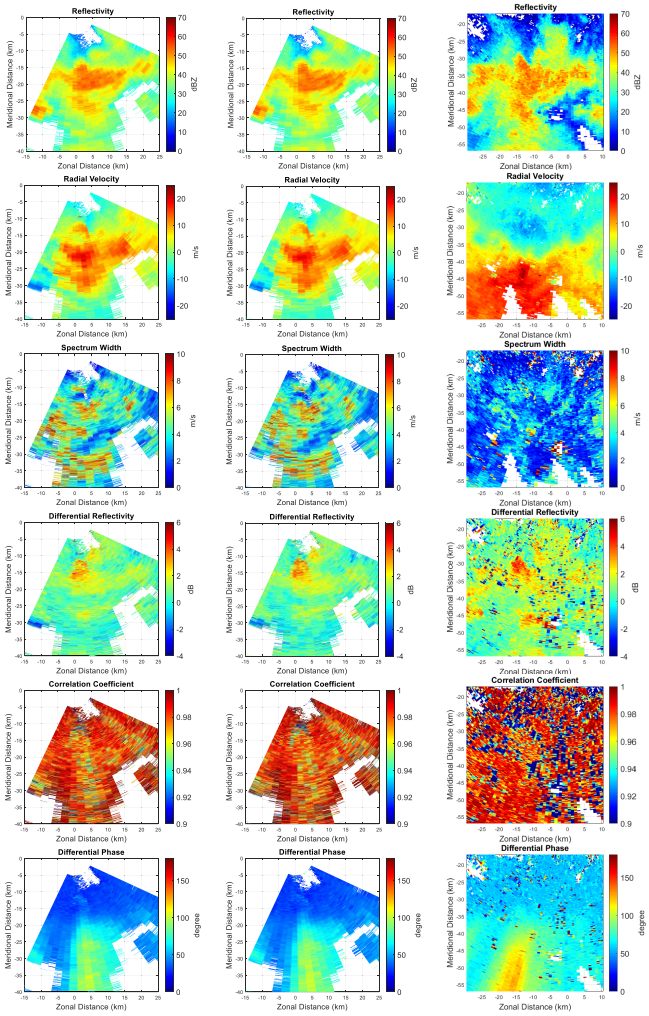

Fig. 5. Weather measurements collected with CPPAR (SNR $\geq$ 5 dB) and KTLX on August 27, 2019. (Left column) CPPAR mechanical scan at 05:03:40 UTC. (Middle column) CPPAR electronic scan at 05:04:04 UTC. (Right column) KTLX mechanical scan at 05:06:10 UTC.

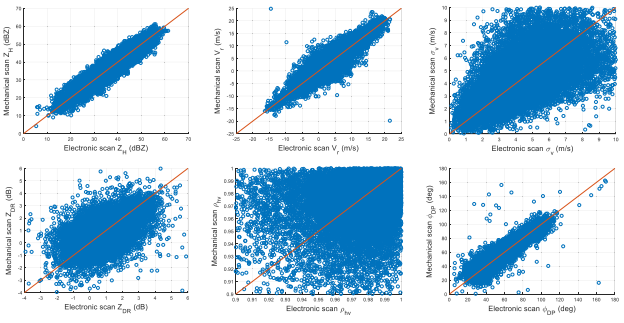

Fig. 6. Scatter plots of CPPAR measurements in precipitation (SNR $\geq$ 5 dB).

CPPAR and KTLX from different radial directions. Furthermore, CPPAR produces higher estimates of σ_{v} due to its wider beam which illuminates more weather scatterers in motion. In addition, one-one scatter plots between CPPAR mechanical scan and electronic scan are shown in Fig. 6.

For further quantitative comparison of CPPAR measurements between electronic scan and mechanical scan, it is more

TABLE II
CPPAR PARAMETERS DURING DATA COLLECTION

Radar Parameters	Mechanical Scan	Electronic Scan
Frequency	2760 MHz	2760 MHz
Waveform	NLFM	NLFM
Pulse Width	34 μs	34 μs
Pulse Repetition Time	1 ms	1 ms
Pulses Per Dwell	64	64
Beam Sectors	1	25
Selected Beam Sector	Columns No.13~36	Columns No.1~24, 2~25, …, 25~48
Rotation Speed	11.75°/s	N/A
Azimuth Sampling Rate	0.75° per dwell	3.75° per dwell
Elevation Angle	3.3°	3.3°

TABLE III
ERROR STATISTICS BETWEEN ELECTRONIC SCAN AND MECHANICAL SCAN OF CPPAR MEASUREMENTS

Moment	Mean Bias	Global STD	Local STD	STD of Estimates	STD in theory
Z_{H} (dBZ)	0.23	2.52	1.54	1.04	0.94
v_{r}(m/s)	-0.15	2.10	1.19	0.80	0.76
σ_{v}(m/s)	-0.04	1.75	0.96	0.63	0.56
Z_{DR}(dB)	-0.01	0.82	0.51	0.36	0.31
ρ_{hv}	0.001	0.021	0.011	0.007	0.007
ϕ_{DP}(deg)	-0.18	5.08	3.16	2.17	1.94

straightforward to reduce noise effects by using high signal-to-noise ratio (SNR) data (see Fig. 8 in [14]), and a threshold of SNR $\geq$ 20 dB was used to filter the raw data for error analysis. Error statistics are shown in Table III, in which the mean bias (MB) and standard deviation (STD) are defined as follows:

$$\mathrm{MB} = \frac{1}{N}\sum_{n=1}^{N}(e_n - m_n) \tag{2}$$

$$\mathrm{STD} = \sqrt{\frac{1}{N}\sum_{n=1}^{N}(e_n - m_n)^2} \tag{3}$$

where e is the measurement value from electronic scan and m is the measurement value from the mechanical scan. It should be noted that the global STD includes two sources of error, in which one comes from random fluctuation due to sampling error, whereas the other results from the inhomogeneity of weather scatterers due to the temporal and spatial difference of the two scans. In this weather case, two CPPAR scans were made with 24 s apart imposed by the scan mode switch time, during which the positions and velocities of weather scatterers in the resolution volume might have changed. To quantify the accuracy of the CPPAR measurements, the random fluctuation due to sampling error is estimated, which is referred to as "local STD." The local STD is estimated from radar estimates over 11 gates (range gate No.1–11, 2–12, 3–13, ...) in each beam, and the corresponding histograms for the electronic scan are shown in Fig. 7. Then, the measured local STD of each radar estimate can be obtained from the median value of the corresponding histogram. In addition, the theoretical STD of radar estimates can also be calculated using the measured median value of σ_{v} and ρ_{hv}, based on the equations in [13] and [15].

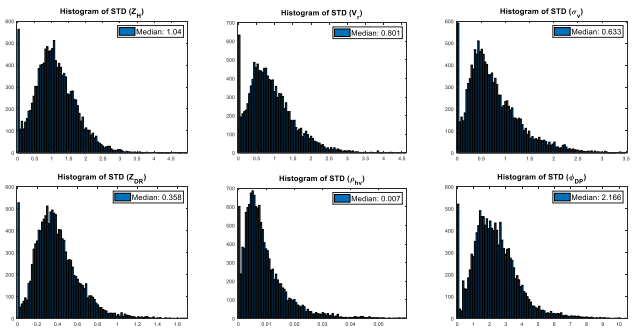

Fig. 7. Histograms of STD of radar estimates in the electronic scan (SNR $\geq$ 20 dB).

As shown in Table III, the STD of the CPPAR estimates (second column from right) and STD in theory (last column) are generally very consistent for electronic scan, which can meet NEXRAD specifications for data quality.

IV. PERFORMANCE COMPARISON OF VARIOUS SCAN MODES IN CLUTTER DETECTION

In weather radar observation, ground clutter will always degrade radar data quality and, hence, affect quantitative precipitation estimation. Therefore, it is important to detect clutter and mitigate its effects as much as possible to ensure accurate weather measurements. Normally, individual stationary ground clutter such as water towers will have very high ρ_{hv}. According to the definition of ρ_{hv} [15]

$$\rho_{\mathrm{hv}} = \frac{\left|\langle n s_{\mathrm{hh}}^{*}(\pi) s_{\mathrm{vv}}(\pi)\rangle\right|}{\left(\langle n|s_{\mathrm{hh}}(\pi)|^2\rangle\langle n|s_{\mathrm{vv}}(\pi)|^2\rangle\right)^{1/2}} \tag{4}$$

where $s_{\mathrm{hh}}(\pi)$ and $s_{\mathrm{vv}}(\pi)$ are backscattering amplitudes for horizontal and vertical polarizations, respectively, and the angular brackets $\langle\cdots\rangle$ denote the ensemble average. The numerator in (4) can be further expanded as follows:

$$\langle n s_{\mathrm{hh}}^{*}(\pi) s_{\mathrm{vv}}(\pi)\rangle = \langle n|s_{\mathrm{hh}}(\pi)||s_{\mathrm{vv}}(\pi)|\rangle e^{-\sigma_\delta^2} e^{j\delta} \tag{5}$$

where the mean scattering phase difference is $\delta = \langle\delta_h - \delta_v\rangle$ which can bias the ϕ_{DP} estimate, and its standard deviation is $\sigma_\delta = \mathrm{STD}(\delta_h - \delta_v)$ which causes decorrelation. Therefore, ρ_{hv} is reduced by a factor of $e^{-\sigma_\delta^2/2}$ due to the random scattering phase difference in the case of melting snow, hail, and biological scatterers, as well as distributed ground clutter [15].

In the mechanical scan mode, there is always the beam smearing effect and the change in the scattering phase difference due to the fast rotation of the antenna, which will increase σ_δ of ground clutter. As a result, the measured ρ_{hv} of ground clutter will be reduced. On the contrary, the commutating scan mode has no beam smearing effect as it electronically steers the beam, and hence, the σ_δ of ground clutter is much lower, which yields the higher ρ_{hv}. This is fundamentally different from the reduced ρ_{hv} for clutter in mechanical scan measurements that we are used to. Therefore, special attention is needed in interpreting electronic PAR measurements.

To validate this theory, ρ_{hv} measured in a clear air condition is compared as follows. As shown in Table II, the azimuth sampling rate is 0.75° per dwell for mechanical scan and 3.75° per dwell for the electronic scan of the CPPAR demonstrator.

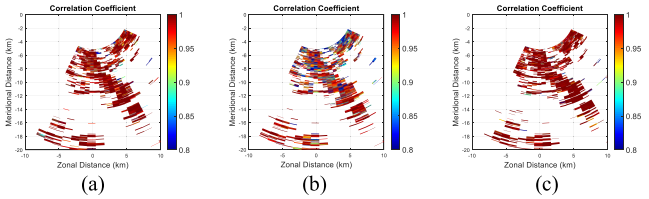

Fig. 8. Comparison of ρ_{hv} under various scan modes in clear air condition. (a) Mechanical scan with a single radial. (b) Mechanical scan with combined radials. (c) Electronic scan.

To make a fair comparison, the azimuth sampling rate should be the same for the two scan modes. A possible solution is to combine every five consecutive radials in the mechanical scan into a new radial, which corresponds to an equivalent azimuth sampling rate of 3.75° per dwell. The processed results are shown in Fig. 8. The measurements in the clear air condition were collected at 01:09:32 UTC for the mechanical scan and 01:09:54 UTC for the electronic scan on August 31, 2019. For comparison purposes, measurements from the mechanical scan processed with the raw single radial are also included. It should be noted that all the results shown in Fig. 8 are before clutter filtering so that the performances of various scan modes in clutter detection can be compared in a fair way.

As shown in Fig. 8, due to the change in differential scattering phase during the scan, ρ_{hv} measured from the mechanical scan with combined radials is obviously lower for ground clutter within 10 km, as shown in blue pixels, compared with that from the electronic scan. As a comparison, ρ_{hv} measured from a mechanical scan with raw single radial shows some reduction but not as serious as the combined beam. The reason is that the azimuth sampling rate of 0.75° per dwell for the mechanical scan is only about one-eighth of the beamwidth of the CPPAR demonstrator, so the change in differential scattering phase of ground clutter during the scan is much smaller.

V. Conclusion

In this letter, initial weather measurements using a CPPAR demonstrator developed at The University of Oklahoma are presented. After a description of technical specifications, waveform design, beam pattern measurement and optimization, and system calibration of the CPPAR demonstrator, weather measurements with single-beam mechanical scan and commutating beam electronic scan, in observation of a convective precipitation, are presented. The measurements are first validated qualitatively with KTLX, and then, the two scan modes are compared quantitatively, and error statistics are derived and discussed. Results show the advantages of the CPPAR's scan-invariant beam characteristics and polarization purity, simplifying the calibration and allowing high-quality polarimetric weather measurements. Moreover, a theoretical explanation of the features of a commutating beam electronic scan in clutter detection that is different from the mechanical scan is presented and confirmed by observations.

Currently, efforts are underway to improve the calibration for the commutating beam electronic scan mode. By obtaining the beam-to-beam stability, the variations in gain and beamwidth among the commutating beams can be mitigated. In addition, advanced signal processing such as multilag correlation estimators will be implemented in CPPAR to further improve the polarimetric data quality.

Acknowledgment

The authors would like to thank the Advanced Radar Research Center (ARRC) Staff Engineers for their dedication to the design and construction of CPPAR.

References

[1] G. Zhang, R. J. Doviak, D. S. Zrnic, J. Crain, D. Staiman, and Y. Al-Rashid, "Phased array radar polarimetry for weather sensing: A theoretical formulation for bias corrections," *IEEE Trans. Geosci. Remote Sens.*, vol. 47, no. 11, pp. 3679–3689, Nov. 2009.

[2] D. S. Zrnic, G. Zhang, and R. J. Doviak, "Bias correction and Doppler measurement for polarimetric phased-array radar," *IEEE Trans. Geosci. Remote Sens.*, vol. 49, no. 2, pp. 843–853, Feb. 2011.

[3] R. J. Doviak, L. Lei, G. Zhang, J. Meier, and C. Curtis, "Comparing theory and measurements of cross-polar fields of a phased-array weather radar," *IEEE Geosci. Remote Sens. Lett.*, vol. 8, no. 5, pp. 1002–1006, Sep. 2011.

[4] L. Lei, G. Zhang, R. J. Doviak, and S. Karimkashi, "Comparison of theoretical biases in estimating polarimetric properties of precipitation with weather radar using parabolic reflector, or planar and cylindrical arrays," *IEEE Trans. Geosci. Remote Sens.*, vol. 53, no. 8, pp. 4313–4327, Aug. 2015.

[5] G. Zhang, R. J. Doviak, D. S. Zrnić, R. Palmer, L. Lei, and Y. Al-Rashid, "Polarimetric phased-array radar for weather measurement: A planar or cylindrical configuration?" *J. Atmos. Ocean. Technol.*, vol. 28, no. 1, pp. 63–73, Jan. 2011.

[6] S. Karimkashi and G. Zhang, "A dual-polarized series-fed microstrip antenna array with very high polarization purity for weather measurements," *IEEE Trans. Antennas Propag.*, vol. 61, no. 10, pp. 5315–5319, Oct. 2013.

[7] S. Karimkashi and G. Zhang, "Optimizing radiation patterns of a cylindrical polarimetric phased-array radar for multimissions," *IEEE Trans. Geosci. Remote Sens.*, vol. 53, no. 5, pp. 2810–2818, May 2015.

[8] C. Fulton *et al.*, "Cylindrical polarimetric phased array radar: Beamforming and calibration for weather applications," *IEEE Trans. Geosci. Remote Sens.*, vol. 55, no. 5, pp. 2827–2841, May 2017.

[9] H. Saeidi-Manesh, M. Mirmozafari, and G. Zhang, "Low cross-polarisation high-isolation frequency scanning aperture coupled microstrip patch antenna array with matched dual-polarisation radiation patterns," *Electron. Lett.*, vol. 53, no. 14, pp. 901–902, Jul. 2017.

[10] J. M. Kurdzo, B. L. Cheong, R. D. Palmer, G. Zhang, and J. B. Meier, "A pulse compression waveform for improved-sensitivity weather radar observations," *J. Atmos. Ocean. Technol.*, vol. 31, no. 12, pp. 2713–2731, Dec. 2014.

[11] M.-H. Golbon-Haghighi, H. Saeidi-Manesh, G. Zhang, and Y. Zhang, "Pattern synthesis for the cylindrical polarimetric phased array radar (CPPAR)," *Prog. Electromagn. Res. M*, vol. 66, pp. 87–98, Mar. 2018.

[12] R. J. Doviak and D. S. Zrnić, *Doppler Radar and Weather Observations*, 2nd ed. New York, NY, USA: Academic, 2006.

[13] V. M. Melnikov and D. S. Zrnić, "Autocorrelation and cross-correlation estimators of polarimetric variables," *J. Atmos. Ocean. Technol.*, vol. 24, no. 8, pp. 1337–1350, Aug. 2007.

[14] Q. Cao, G. Zhang, R. D. Palmer, M. Knight, R. May, and R. J. Stafford, "Spectrum-time estimation and processing (STEP) for improving weather radar data quality," *IEEE Trans. Geosci. Remote Sens.*, vol. 50, no. 11, pp. 4670–4683, Nov. 2012.

[15] G. Zhang, *Weather Radar Polarimetry*. Boca Raton, FL, USA: CRC Press, 2016.